Available online at www.sciencedirect.com
ScienceDirect
Combustion and Flame 151 (2007) 649–664
Combustion and Flame
www.elsevier.com/locate/combustflame

Numerical and experimental investigation of a mild combustion burner

Chiara Galletti *, Alessandro Parente, Leonardo Tognotti

Department of Chemical Engineering, Industrial Chemistry and Materials Science, University of Pisa, via Diotisalvi 2, 56126 Pisa, Italy

Received 22 November 2006; received in revised form 25 May 2007; accepted 17 July 2007

Available online 4 October 2007

Abstract

An industrial burner operating in the MILD combustion regime through internal recirculation of exhaust gases has been characterized numerically. To develop a self-sufficient numerical model of the burner, two subroutines are coupled to the CFD solver to model the air preheater section and heat losses from the burner through radiation. The resulting model is validated against experimental data on species concentration and temperature. A 3-dimensional CFD model of the burner is compared to an axisymmetric model, which allows considerable computational saving, but neglects some important burner features such as the presence of recirculation windows. Errors associated with the axisymmetric model are evaluated and discussed, as well as possible simplified procedures for engineering purposes. Modifications of the burner geometry are investigated numerically and suggested in order to enhance its performances. Such modifications are aimed at improving exhaust gases recirculation which is driven by the inlet air jet momentum. The burner is found to produce only 30 ppm_v of NO when operating in MILD combustion mode. For the same air preheating the NO emissions would be of approximately 1000 ppm_v in flame combustion mode. It is also shown that the burner ensures more homogeneous temperature distribution in the outer surfaces with respect to flame operation, and this is attractive for burners used in furnaces devoted to materials' thermal treatment processes. The effect of air excess on the combustion regime is also discussed.

Keywords: MILD combustion; Flameless; Burner; CFD

1. Introduction

The improvement of combustion efficiency to reduce fossil fuel consumption and carbon dioxide emission is a key issue in combustion research. Therefore, the achievement of high-energy-efficiency processes through advanced heat recovery systems is desirable even if the increase in process temperature arising from air preheating generally leads to very large NO_x emissions. However, NO_x emissions are regulated in many countries with increasingly stringent laws because of their adverse impact on the environment (climate change, acid rains, photochemical smog). Thus, the development of a combustion technology able to accomplish large energy savings with very low pollutant emissions has become a primary concern.

* Corresponding author. Fax: +30 050511266.
E-mail address: chiara.galletti@ing.unipi.it (C. Galletti).

0010-2180/$ – see front matter
doi:10.1016/j.combustflame.2007.07.016

Nomenclature

A	area	m^2
$A_{air,in}$	air inlet cross-sectional area	m^2
Da	Damkohler number	–
e	emissivity	–
e_{air}	air excess	–
F	view factor	–
k_{ins}	insulation layer thermal conductivity	$W\,m^{-1}\,K^{-1}$
k_{prompt}	kinetic constant of prompt NO	s^{-1}
k_R	recirculation degree of burnt gases into the reaction region	%
k_{R0}	parameter in Eq. (12)	–
$k_{thermal}$	kinetic constant of thermal NO	$m^{1.5}\,K^{0.5}\,mol^{-0.5}\,s^{-0.5}$
$\bar{k}(T)$	kinetic constant integrated over a PDF of temperature, arbitrary units	
L_{em}	emitter length	m
$\dot{m}$	mass flow rate	$kg\,s^{-1}$
PDF(T)	probability density function	–
$\dot{Q}$	irradiative heat flux	W
$\dot{Q}_{in}$	burner load	W
$\dot{Q}_{rec}$	heat flux exchanged in the air preheater	W
r	radial coordinate	m
R	radius	m
T	temperature	K
$\dot{w}$	reaction rate	$kg\,m^{-3}\,s^{-1}$
W	molecular weight	$kg\,mol^{-1}$
x	axial coordinate	m
X	molar fraction	–
[ ]	molar concentration	$mol\,m^{-3}$

Greek symbols

η	efficiency	–
ρ	density	$kg\,m^{-3}$
σ	Boltzmann constant, $\sigma = 5.67 \times 10^{-8}\,W\,m^{-2}\,K^{-4}$	
τ_c	chemical timescale	s
τ_t	turbulent timescale	s

Subscripts

1	radiant tube
2	Inconel shield
2′	internal insulation layer of the Inconel shield
2″	external insulation layer of the Inconel shield
3	water heat exchanger
A	air
EG	exhaust gases
F	fuel
max	maximum
mix	mixture
rad	radiant tube
reaction	reaction region
rec	heat recovery section
Δk	parameter in Eq. (12)

In this framework, MILD combustion appears interesting, as it may ensure high combustion efficiencies with low pollutant emissions [1,2].

Such a combustion regime needs the reactants to be preheated above the self-ignition temperature and enough inert combustion products to be entrained in the reaction region. The former requirement ensures high thermal efficiency, whereas the latter allows diluting the flame and reducing the final temperature well below the adiabatic flame temperature. As a result, a flame front is no longer identifiable, so that MILD combustion is often denoted as flameless combustion. Moreover, it has been observed that ignition and extinction phenomena do not occur in MILD combustion because of the small temperature difference between burnt and unburnt gases.

Among the advantages associated with this combustion technology, one is that flame stabilization occurs naturally as the reactants' temperature exceeds the self-ignition temperature. Therefore a large degree of freedom in the choice of the fluid dynamical configuration of the combustion chamber is allowed. Moreover, the temperature field homogeneity and reduced gradients allow better control of maximum temperatures with beneficial effects on materials.

Importantly, NO_x emissions are greatly reduced because of the limited temperature increase. Soot formation is also suppressed, because of the lean conditions in the combustion chamber, due to the large dilution levels. In addition, the large CO_2 concentration due to the recirculation of combustion products has a beneficial effect of soot suppression [2].

Therefore, MILD combustion poses itself as a technology combining high efficiencies, because of the strong preheating, with low pollutant emissions.

All these aspects make MILD combustion worthy of further investigations and attention, even though, to date, several studies have been devoted to understanding its operational conditions [3] as well as its mechanisms and critical parameters [4]. An extensive review on MILD combustion features considering physical, chemical, and thermodynamic aspects has been provided by Cavaliere and de Joannon [2].

From a technological point of view, the first requirement for MILD combustion, reactant temperature above the self-ignition temperature, may be

achieved by preheating the fuel, the oxidizer, or both. The second requirement, large entrainment of inert species in the reaction region, may be achieved in different ways by either internal or external recirculation of exhaust gases.

MILD combustion burners appear well suited for those industrial processes that require a high and homogeneous temperature distribution within the combustion chamber (e.g., in the glass and ceramic industry, in steel thermal treatments). For these processes, energy recovery represents a primary issue to ensure acceptable energy efficiency; consequently, the use of MILD combustion seems to be particularly beneficial [1]. Energy saving can be achieved with either recuperative or regenerative burners according to the heat exchanger area and the preheating rate required. These burners are usually designed to operate both in flame and in MILD mode by varying the reactants' feeding mode. The combination of recuperative MILD combustion burners with radiant tubes is a widely applied solution in many thermal treatments of material surfaces, to avoid any contact or contamination of the flue gases with the stock surface to be treated [5].

Choi and Katsuki [6] investigated the feasibility of flameless oxidation in industrial glass furnaces. They found that the combustion process was sustained even with low-calorific-value fuels and low oxygen concentrations if the combustion air was preheated above the fuel self-ignition temperature. Results also showed that NO_x formation was controlled by the mixing process between fuel and the preheated air.

Flamme [7] investigated the application of MILD combustion to glass melting furnaces operating with a process temperature around 1600 °C and air preheating temperatures up to 1350 °C. Experimental results on a 300-kW furnace showed that the replacement of conventional burners with recuperative MILD combustion burners lead to dramatic reduction of NO_x emission, from 1500 ppm_v down to values safely below 100 ppm_v.

The application of MILD combustion in different fields than thermal treatment processes is also very attractive. The advantages of a clean and quiet combustion process could be exploited in several fields of application, including power generation, micro cogeneration, and low-temperature applications.

Flamme [8] showed the applicability of recuperative MILD combustion burners to gas turbines in overcoming the oscillation problems typical of lean premixed combustion occurring in gas turbines. Recently Wang et al. [9] performed a technical, environmental, and economic analysis of NO_x reduction technologies at a gas turbine power station. Results showed that the use of recuperative MILD combustion burners could offer an effective method for reducing NO_x emissions, the technology being much cheaper than SCR and requiring only a slight increase in capital cost and electricity selling price with respect to the simple cycle gas turbine power plants.

Also, the homogeneous charge compression ignition (HCCI) engines are based on a concept that may be included in MILD combustion [2]. HCCI engines achieve a homogeneous charge in the combustion chamber at such a high compression ratio that self-ignition occurs homogeneously in the entire chamber. Under this condition the mixture temperature is higher than the self-ignition temperature; however, the maximum temperature is kept low by means of a superlean mixture and/or inert dilution. With such condition, very little NO_x is produced and relatively high-efficiency cycles can be designed.

Given the industrial interest, recently increasing attention has been paid not only to the experimental characterization of MILD combustion burners, but also to their modeling through computational fluid dynamics (CFD). In particular, CFD may help in optimizing burners' performances by investigating geometrical details, such as injection nozzles' configurations and internal devices for flue gas recirculation. Moreover, data on lab-scale burners are difficult to transfer to industrial burners operating in MILD combustion, as the usual scaling criteria are no longer adequate. Indeed, the CFD support is desirable [10].

Some attempts at modeling MILD combustion operation have been proposed and some criteria and hints have been suggested, even if there is still not a unique response.

Actually, despite the flame homogeneity and smooth gradients occurring in this combustion mode, MILD combustion appears more difficult to model than conventional flames, e.g., premixed or diffusion flames, because the high dilution levels and the relatively low temperatures lower the chemical reaction rates, making them comparable to turbulent mixing phenomena, which are enhanced by recirculation. Therefore the turbulence–chemistry interaction treatment becomes a crucial point in the modeling procedure.

Coelho and Peters [11] simulated a furnace operating in the MILD combustion mode by applying the flamelet approach to describe turbulence/chemistry interactions. They compared predictions with measurements supplied by Plessing et al. [12] and Özdemir and Peters [13]. Although a qualitative agreement between the experimental and predicted flow field was observed, some considerable discrepancies were present. In addition the residence time was underestimated by the numerical model, and the flamelet approach was found to be unable of describing correctly

the NO formation. Better results could be achieved by means of the unsteady flamelets [14].

Orsino et al. [15] investigated the performance of three combustion models (eddy break-up, eddy dissipation concept with chemical equilibrium, and PFD/mixture fraction) for predicting the combustion of natural gas with high-temperature air and large quantities of flue gas and found that all models failed in the vicinity of the fuel injection. However the authors claimed that they could obtain excellent NO predictions through the steady flamelet library.

Recently, Christo and Dally [16] pointed out difficulties arising when modelling MILD combustion burners. They investigated numerically a jet in hot coflow burner replicating MILD combustion regime. The burner was characterised experimentally by Dally et al. [17]. The authors used different turbulence, combustion, and kinetic models, comparing their performance. In particular they showed that mixture fraction/probability density function and flamelet approaches perform poorly for the MILD combustion regime. The eddy dissipation model also gave unsatisfactory results. Better predictions were achieved through combustion models considering both chemistry and turbulence effects, such as the eddy dissipation concept of Magnussen and Hjertager [18]. In addition, the aforementioned authors observed that molecular diffusion may play an important role in MILD combustion: for instance, the predicted temperatures were higher than the measured ones by approximately 10% if differential diffusion effects were neglected. It is worth noting that the general view in turbulent flames modelling is to neglect the molecular diffusion term and to take into account only turbulent diffusion.

In the present work, a numerical model of an industrial burner operating in MILD combustion is validated against experimental data. Local measurements across the combustion chamber could not be performed because the industrial burner does not allow any access to its interior; however, efforts were made to characterize the burner behavior through as many measurements as possible (for instance, by measuring temperatures along the outer surfaces of the burner). The proposed numerical model contains two subroutines able of representing the recuperative section behavior and the heat exchanges between the burner and the surroundings. These subroutines were necessary in order to avoid any assumption in the burner modeling. In addition, two models of the burner have been investigated: a 3-dimensional model, which replicates the real burner features, and an axisymmetric model. The axisymmetric model has been investigated as this model is commonly adopted [19,20] because of the low computational cost. However the axisymmetric model neglects some burner features that could considerably affect the fluid dynamical behavior of the burner and, subsequently, predictions. Ultimately, burner geometry modifications and effects of some operational conditions (e.g., air excess) on the burner behavior are numerically analyzed.

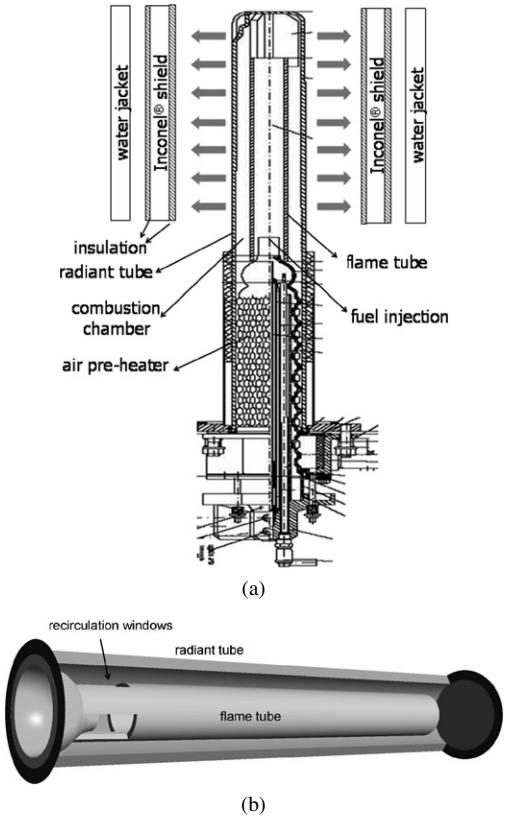

Fig. 1. (a) Longitudinal section of the burner and (b) 3-dimensional view of the combustion chamber.

2. The burner

The burner is a recuperative MILD combustion burner with a nominal power of 13 kW and belongs to ENEL Ricerca. A longitudinal section of the burner is reported in Fig. 1a. The combustion chamber is delimited by a radiant tube closed at the upper end. Indeed, the burner is suited for all applications where the combustion environment has to be kept separated from the media to be heated (e.g., furnaces for steel annealing processes, glass making). The combustion chamber is cylindrical with a radius of 0.045 m and a length of 0.58 m. It operates with an internal recirculation of exhaust gases which is promoted by a 0.41-m-long flame tube with a radius of 0.02 m positioned inside the burner. The flame tube is equipped with three windows in the lower part which allow the recirculation of exhaust gases in the reaction region.

A 3-dimensional view of the combustion chamber with the recirculation windows is depicted in Fig. 1b.

Outside the combustion chamber, and coaxial to the radiant tube, an Inconel shield and a water heat exchanger were placed in the experimental apparatus to replicate heat losses toward the surrounding of real burner operations. Two insulation layers covered the inner and outer surfaces of the Inconel shield (see Fig. 1a).

Importantly, the burner is self-recuperative, which means that the inlet air is preheated with exhaust gases by means of a finned-surface heat exchanger (see the lower part of Fig. 1a).

The burner can work in either flame or MILD combustion mode. Initially, the combustion chamber should be heated up with a flame combustion mode, as MILD combustion requires temperatures higher than the self-ignition temperature of the fuel. Once the high temperatures are reached, the burner switches from flame to MILD combustion mode.

Fuel and air are fed into the combustion chamber through separated jets. In particular, the fuel is injected on the burner axis, whereas the air is fed from an outer annulus in a co-flow configuration. In this manner the fresh air can entrain large amounts of burnt gases before reacting with the fuel.

Measurements were made of the composition of exhaust gases as well as temperatures along the radiant tube and the Inconel shield, both of them equipped with series of thermocouples.

Experimental runs are listed in Table 1 (see runs 1–7). Different burner loads were investigated by varying the fuel flow rate and air excess.

3. Numerical model

The numerical simulations were performed with the commercial code CFX 5.7 by Ansys Inc.

It can be observed from Table 1 that runs 1–7 were investigated both numerically and experimentally, whereas runs 8–14 were analyzed only numerically. These latter runs were partly aimed at investigating burner geometry modifications (runs 8–12) and the influence of air excess (runs 13–14) on the burner behavior.

In particular, the air inlet cross-sectional area was varied from 339 down to 41 mm^2, in order to change the recirculation degree of exhaust gases, such recirculation being driven by the momentum of the air inlet jet. Actually, the real burner operates with just one air inlet cross-sectional area, 88 mm^2. Values of $A_{air,in}$ for each run are listed in the fifth column of Table 1.

The air excess was varied from 40 to 46%, which characterizes the experimental campaign and ensures an oxygen concentration of about 6% in the exhaust gases, down to 16%, corresponding to an oxygen concentration of about 2.6% in the exhaust gases.

3.1. Computational domain and grid

The computational domain consisted of three subdomains: a fluid domain representing the real combustion chamber and two solid domains representing the flame and the radiant tubes. It was chosen to simulate those two solid subdomains to take into account heat exchanges, due mainly to radiation effects between the reacting gas and the solid boundaries. Besides, the radiant tube modeling was done on purpose to allow a comparison between predictions and experimental data obtained from the thermocouples mounted along the radiant tube.

Because of the presence of three recirculation windows, a 120° angular sector was modeled. The grid contained 350,000 cells and consisted of parts meshed with tetrahedra (near burner zone) and parts

Table 1
Experimental and numerical runs investigated

Run	$\dot{Q}_{in}$ (kW)	$\dot{m}_F$ (kg/s)	e_{air} (%)	A_{air_in} (mm^2)	k_R (%)	$C/O_{reaction}$ (–)	$X_{O_2,reaction}$ (–)	Exp.	CFD	CFD model
1	8.23	1.72E–04	60	88	130	0.105	0.126	X	X	3D
2	9.13	1.90E–04	44	88	138	0.122	0.117	X	X	3D
3	9.31	2.38E–04	40	88	137	0.128	0.115	X	X	3D
4	9.9	2.55E–04	40	88	134	0.129	0.115	X	X	3D
5	10.53	2.70E–04	44	88	135	0.120	0.118	X	X	3D
6	10.7	2.73E–04	40	88	134	0.129	0.115	X	X	3D
7	10.42	2.67E–04	46	88	136	0.120	0.119	X	X	2D, 3D
8	10.42	2.67E–04	46	339	23	0.160	0.171		X	2D, 3D
9	10.42	2.67E–04	46	201	59	0.144	0.146		X	2D, 3D
10	10.42	2.67E–04	46	64	173	0.111	0.111		X	2D, 3D
11	10.42	2.67E–04	46	46	200	0.105	0.106		X	2D, 3D
12	10.42	2.67E–04	46	41	235	0.098	0.102		X	2D, 3D
13	10.42	2.67E–04	16	88	128	0.183	0.099		X	3D
14	10.42	2.67E–04	16	41	223	0.165	0.078		X	3D

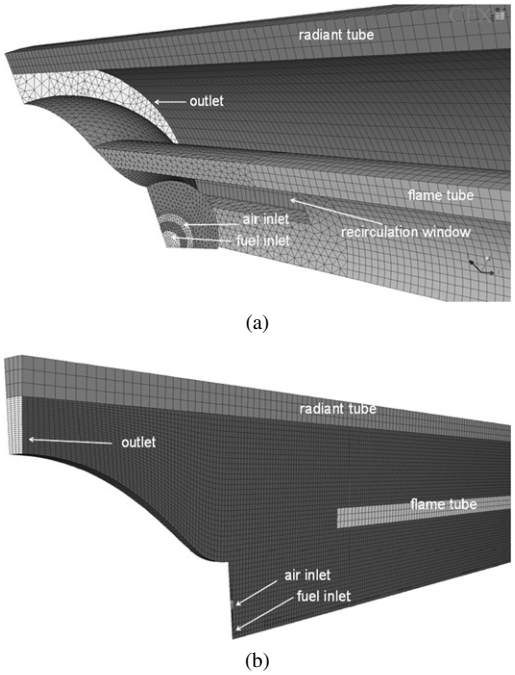

Fig. 2. (a) 3-Dimensional and (b) axisymmetric grids.

meshed with hexahedra (reaction and reverse flow zone, flame tube and radiant tube). Specifically there were 143,000 tetrahedra and 207,000 hexahedra. The choice of a hybrid grid was aimed at reducing the number of cells required to discretize the computational domain accurately. Tetrahedra were required to properly characterize some burners' features, e.g., recirculation windows; however, a grid constituted only of tetrahedra would have been characterized by a huge number of cells. The computational grid is shown in Fig. 2a.

Some simulations were also performed with the axial symmetry hypothesis, thus neglecting the presence of the recirculation windows. In other words, in these simulations the recirculation area corresponded to the whole annulus comprised between the lower part of the burner and the flame tube; consequently the recirculation area is larger than that considered with the 3D model. This was done on purpose to evaluate the effect of recirculation windows; nevertheless, simulations available in the literature of recuperative MILD combustion burners are usually 2D simulations [19,20]. The axisymmetric model is shown in Fig. 2b. The structured grid consisted of 120,000 hexahedra, arranged in four layers describing an angular sector of 5°.

A grid independence study was carried out on both the 3D and the axisymmetric models. The effect of mesh refinement and coarsening was investigated by doubling and halving the number of elements of the actual mesh used in the computations and comparing the radial profiles of temperature and major species at different axial locations along the burner.

3.2. Boundary conditions

As far as boundary conditions are concerned, fuels were fed at room temperature (298 K). Conversely, the air inlet temperature was evaluated as a function of exhaust gas temperature, on the basis of experimental data on the air preheater available from the burner supplier. A model was developed from experimental data fitting and implemented through a subroutine in the code; as a result, the air inlet temperature was adjusted on the basis of the exhaust gas temperature.

As mentioned earlier, special attention was paid to the boundary conditions of the radiant tube, as some of the available experimental data regarded this region. Heat is lost from the radiant tube toward the Inconel shield by radiation, and subsequently heat is conducted through the Inconel shield and the two insulation layers covering it; ultimately heat is transferred from the shield to the water heat exchanger through radiation.

A subroutine based on conduction and radiation between coaxial cylindrical shields was written on purpose to evaluate the heat losses from the radiant tube. The irradiative heat flux between radiant tube (1) and inner insulation layer ($2'$) is

$$\dot{Q}_{12'} = e_{12'}\sigma A_1\left(T_1^4 - T_{2'}^4\right), \tag{1}$$

where $e_{12'} = \dfrac{1}{\frac{1-e_1}{e_1} + \frac{1}{F_{12'}} + \frac{R_1}{R_{2'}}\left(\frac{1-e_{2'}}{e_{2'}}\right)}$.

The conductive heat transfer within the insulation layers $2'$ and $2''$ is given by

$$\dot{Q}_{12'} = \frac{2\pi L_{\mathrm{em}} k_{\mathrm{ins}}(T_{2'} - T_{2''})}{\ln(R_{2''}/R_{2'})}, \tag{2}$$

neglecting the thermal resistance of the Inconel shield.

The irradiative heat flux between the outer insulation layer ($2''$) and the water heat exchanger (3) is

$$\dot{Q}_{2''3} = e_{2''3}\sigma A_{2''}\left(T_{2''}^4 - T_3^4\right), \tag{3}$$

where

$$e_{2''3} = \frac{1}{\frac{1-e_{2''}}{e_{2''}} + \frac{1}{F_{2''3}} + \frac{R_{2''}}{R_3}\left(\frac{1-e_3}{e_3}\right)}.$$

In the above equations T_1 is the radiant tube temperature and T_3 is the water heat exchanger temperature, i.e., $T_3 = 323$ K, whereas $T_{2'}$ and $T_{2''}$ are the temperatures of the inner and outer insulation layers respectively. e_1, $e_{2'}$, $e_{2''}$, and e_3 are the emissivities of the radiant tube, the inner and outer insulation layers of the Inconel shield, and the water heat exchanger,

respectively. L_{em} is the emitter length, i.e., the length of the coaxial shield radiating toward the surroundings, whereas k_{ins} is the thermal conductivity of the insulation layers. $F_{12'}$ and $F_{2''3}$ are the view factors between coaxial cylinders; thus their values were set equal to 1 (neglecting radiation losses towards the burner axis).

Such a value is strictly correct for infinite length cylinders; however, this was considered an adequate approximation because the radiant tube, the Inconel shield, and the water heat exchanger have a length much greater than their radius.

At steady state $\dot{Q}_{12'} = \dot{Q}_{2'2''} = \dot{Q}$; consequently the following expression for $\dot{Q}$ is obtained by expressing $T_{2'}$ and $T_{2''}$ as a function of T_1 and T_3:

$$\dot{Q} = \frac{1}{\left(\frac{1}{\sigma e_{12'} A_1} + \frac{1}{\sigma e_{2''3} A_2}\right)} \times \left\{ T_1^4 - T_3^4 + \left[\left(T_1^4 - \frac{\dot{Q}}{\sigma e_{12'} A_1} \right)^{0.25} - \frac{\dot{Q}}{\frac{2\pi L_{em} k_{ins}}{\ln R_{2''}/R_{2'}}} \right]^4 - \left(T_1^4 - \frac{\dot{Q}}{\sigma e_{12'} A_1} \right) \right\}. \quad (4)$$

Equation (4) made necessary an iterative procedure to solve the heat flux $\dot{Q}$.

It may be argued that a discretization of the radiant tube and the outer cylinders would led to a more accurate evaluation of radiation losses. However, the temperature gradients along the radiant tube were not high enough to justify the higher computational cost required by this approach.

3.3. Physical model

Favre-averaged Navier–Stokes equations were solved by using a modified version of the k–ε turbulence model. The first constant of the dissipation transport equation $C_{\varepsilon 1}$ was set equal to 1.6 instead of 1.44 as suggested by Morse [21] in order to overcome the deficiency of the standard k–ε model in predicting round jets properly.

The combined eddy dissipation model/finite rate chemistry (EDM/FRC) was chosen as combustion model. Such a model calculates both a chemical Arrhenius rate and a turbulent mixing rate based on the Magnussen–Hjertager equation and then chooses the lower of the two rates to be inserted in the species' transport equation. The EDM/FRC approach was considered well suited for modeling MILD combustion. As mentioned previously, the conditions of elevated and uniform temperature distribution and low oxygen concentration, which characterize the MILD combustion regime, lead to slower reaction rates with respect to conventional combustion regimes and enhance the influence of molecular diffusion on flame characteristics.

The discrete transfer radiation model was used with a number of rays equal to 16. A coarsening rate equal to 24 was applied to the actual grid to facilitate the radiation calculation. Some simulations were also made with the Monte Carlo model, but as results differed by less than 5%, the former model was preferred because of its lower computational cost.

The radiation properties of the reacting mixture were taken into account with the weighted-sum-of-gray-gases (WSGG) model using the coefficients proposed by Smith et al. [22]. This model was applied by coupling the code with a subroutine written on purpose.

As far as the kinetic mechanism is concerned, a simple one-step global mechanism was used for the methane oxidation [23],

$$CH_4 + 2O_2 \xrightarrow{\dot{w}_{CH_4}} CO_2 + 2H_2O, \quad (5)$$

with

$$\dot{w}_{CH_4} = W_{CH_4} 8.3 \times 10^5 \exp\left(-\frac{15{,}100\ \mathrm{K}}{T}\right) \times [CH_4]^{-0.3} [O_2] \left(\frac{\mathrm{kg}}{\mathrm{m^3\,s}}\right).$$

Thermal NO formation was modeled with a finite rate chemistry combustion (FRC) model and a simplified one-step kinetic mechanism, available in the code. The simplified mechanism is obtained from the Zeldovich scheme by assuming a steady state for the N radicals and relating the O radical concentration to that of oxygen by means of the dissociation reaction [24]. The resulting rate is expressed as

$$\dot{w}_{NO,thermal} = W_{NO} k_{thermal} [O_2]^{1/2} [N_2] \left(\frac{\mathrm{kg}}{\mathrm{m^3\,s}}\right), \quad (6)$$

where

$$k_{thermal} = \frac{4.52 \times 10^{15}}{\sqrt{T}} \exp\left(-\frac{69{,}466\ \mathrm{K}}{T}\right) \left(\frac{\mathrm{m^3\,K}}{\mathrm{kmol\,s^2}}\right)^{1/2}.$$

The prompt NO formation from methane was modeled using a similar approach, according to the one-step mechanism proposed by De Soete [25],

$$\dot{w}_{NO,prompt} = W_{NO} k_{prompt} [O_2]^{1/2} [N_2][F] \times \left(\frac{W_{mix}}{\rho}\right) \left(\frac{\mathrm{kg}}{\mathrm{m^3\,s}}\right), \quad (7)$$

where

$$k_{prompt} = 1.2 \times 10^6 \exp\left(-\frac{30{,}215\ \mathrm{K}}{T}\right) \left(\frac{1}{\mathrm{s}}\right).$$

For both thermal and prompt NO formations, the Arrhenius equation was integrated over a probability density function (PDF) for temperature in order to take into account turbulence effects,

$$\bar{k}(T) = \frac{1}{T_{\max} - T_{\min}} \int_{\min}^{\max} k(T) P(T)\, dT, \tag{8}$$

where $T_{\max} - T_{\min}$ is the temperature range of interest and PDF(T) is the probability density function that is computed from the mean temperature and the variance of the temperature. The shape of the PDF(T) is presumed to be a two-moment β-function as appropriate for combustion calculations [26]. Equation (8) must be integrated at every grid node and at every iteration. The limits of integration are determined from the minimum and maximum values of temperature in the combustion solution.

The implementation of detailed NO formation mechanisms is in progress.

Molecular diffusion effects were taken into account with the Slattery and Bird [27] equation for binary diffusion coefficients. The molecular species were assumed to diffuse in a mixture manly constituted by nitrogen, due to the large amount of inert gases recirculating in the reaction zone. This approximation was found to be consistent with results obtained from a more rigorous approach, consisting in the evaluation of the effective mass diffusivities for the species diffusing in the gas mixture by applying the Wilke mixing rule [28] to the binary diffusion coefficients obtained from the Slattery and Bird equation [27]. Thus, the former approximation was preferred due to the much lower computation cost.

However, simulations performed with and without taking into account molecular diffusion showed that for the investigated cases the effect of molecular diffusion is negligible with respect to turbulent diffusion.

4. Results

4.1. Assessment of the numerical model

First, CFD simulations were validated against experimental data. This is a necessary operation, as the CFD model of the burner is rather complex, containing two subroutines for the air preheater modeling and the calculation of heat exchanges between the burner and surroundings (see Section 3.2).

Fig. 3 shows the comparison between predicted and measured temperatures along the radiant tube for two different experimental runs (runs 1 and 2 of Table 1). The agreement is satisfactory, as the temperature predicted profiles fit measured data well. This confirms that the representation of radiation losses through a model based on radiation between coaxial cylindrical shields was somewhat appropriate, despite the approximations behind the model.

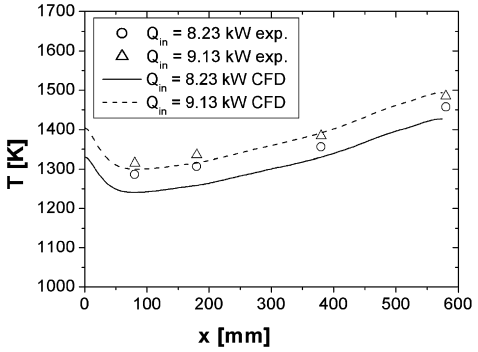

Fig. 3. Comparison between predicted and measured temperatures along the radiant tube for runs 1 and 2.

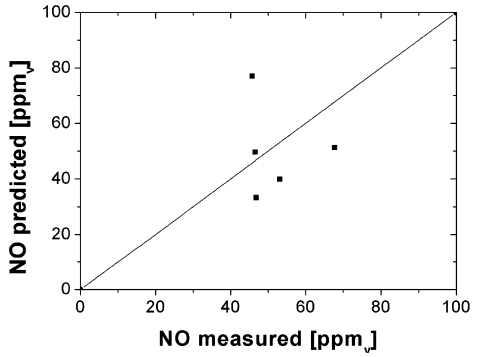

Fig. 4. Comparison between predicted and measured NO emissions normalized to 3% oxygen in the flue gases.

The parity plot of Fig. 4 shows the comparison between experimental and predicted NO emissions. NO concentrations have been normalized to 3% of oxygen in the exhaust gases in order to compare the different runs, these being characterized by different air excesses. It can be observed an acceptable agreement between predicted and measured data, although kinetics of NO formation were rather simple.

4.2. Effect of increasing air inlet velocity

The flow pattern in the burner confirms the mechanism that promotes the exhaust gases recirculation. The burnt gases are entrained by the fresh air jet and deviated from their path, so that they recirculate toward the combustion zone.

The degree of recirculation can be evaluated with the recirculation factor, defined as $k_R = \dot{m}_{EG}/(\dot{m}_B + \dot{m}_A)$, where $\dot{m}_{EG}$ is the mass flow rate of the exhaust gases recirculating into the reaction zone. k_R was found to increase when the air inlet cross-sectional area was reduced, varying between $k_R = 23\%$ with

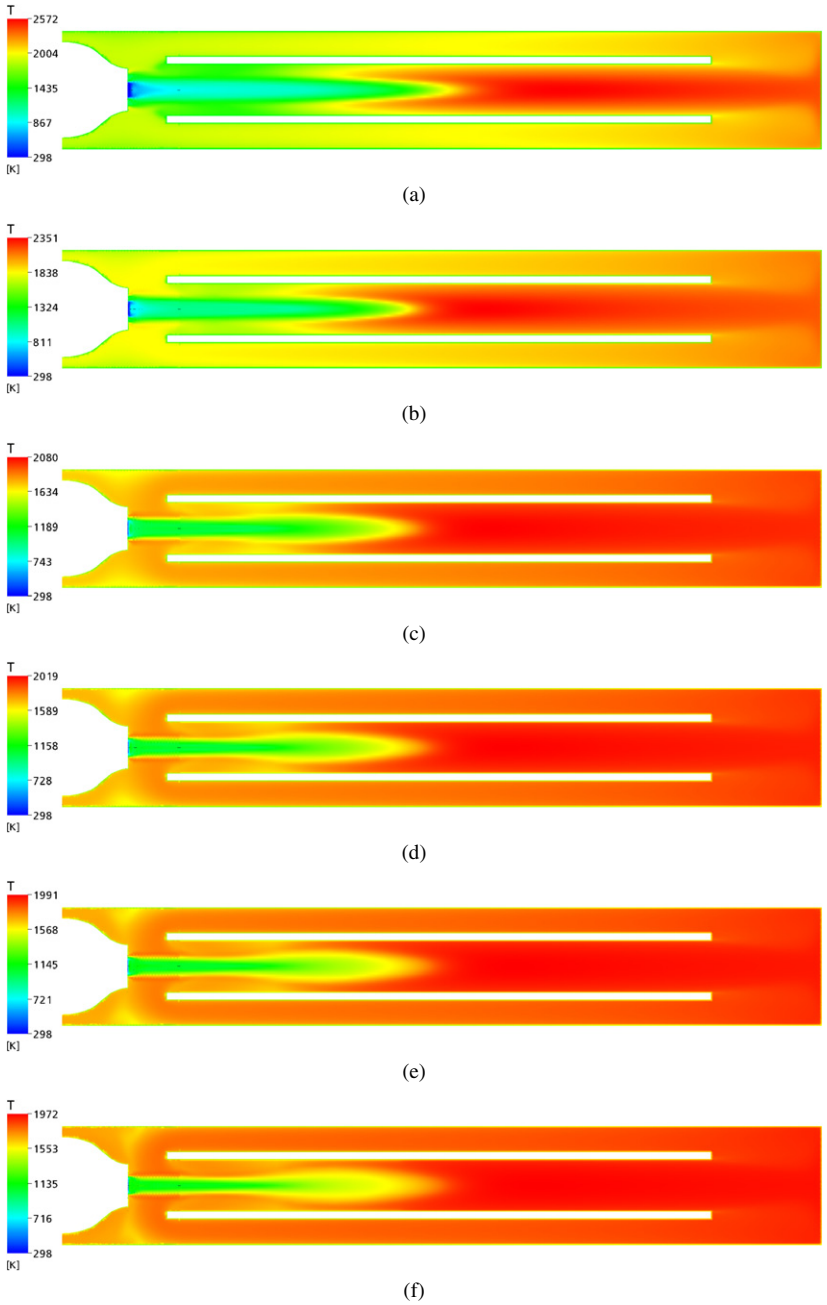

Fig. 5. Temperature distribution for (a) $A_{\mathrm{air,in}} = 339\ \mathrm{mm}^2$; (b) $A_{\mathrm{air,in}} = 201\ \mathrm{mm}^2$; (c) $A_{\mathrm{air,in}} = 88\ \mathrm{mm}^2$; (d) $A_{\mathrm{air,in}} = 64\ \mathrm{mm}^2$; (e) $A_{\mathrm{air,in}} = 46\ \mathrm{mm}^2$; (f) $A_{\mathrm{air,in}} = 41\ \mathrm{mm}^2$. $\mathrm{Burner}_{\mathrm{load}}$ $\dot{Q}_{\mathrm{in}} = 10.42$ kW (runs 7–12 of Table 1).

$A_{\mathrm{air,in}} = 339\ \mathrm{mm}^2$ and $k_{\mathrm{R}} = 235\%$ with $A_{\mathrm{air,in}} = 41\ \mathrm{mm}^2$, for the 10.42-kW burner loads (runs 7–12 of Table 1). The real burner operates with $A_{\mathrm{air,in}} = 88\ \mathrm{mm}^2$, thus with a recirculation degree of $k_{\mathrm{R}} = 136\%$. Values of k_{R} for each run are listed in the sixth column of Table 1. Moreover, the seventh and eighth columns of the table report the C/O ratio and the O_2 molar fraction in the reaction region, respectively. It can be observed that the C/O ratio is rather low, but this is partly imputed to the relatively large air excesses used in the experimental runs.

Fig. 5 shows the temperature distributions in the burner for different recirculation degrees. A more homogeneous temperature distribution can be seen in the burner with increasing recirculation degree.

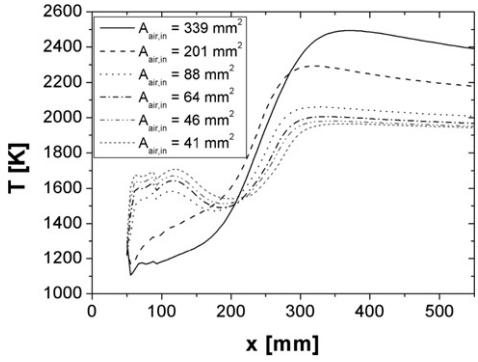

Fig. 6. Axial temperature profiles at $r = 7$ mm for different air inlet cross-sectional areas. Burner load $\dot{Q}_{in} = 10.42$ kW (runs 7–12 of Table 1).

The maximum temperatures observed in the burner were found to be reduced by more than 100 K when the air inlet cross-sectional area was halved, from $T_{max} = 2080$ K for $k_R = 136\%$ down to $T_{max} = 1972$ K for $k_R = 235\%$. Simulations performed with air inlet cross-sectional areas larger than the real one exhibited high-temperature peaks of 2572 and 2351 K for $k_R = 23\%$ and $k_R = 59\%$, respectively. In addition, these predictions indicated the presence of a flame front; thus the burner was operating in flame rather than in MILD combustion conditions.

Fig. 6 illustrates axial profiles of temperature at a radial distance $r = 7$ mm and for different air inlet cross-sectional areas. The radial distance $r = 7$ mm was chosen as it corresponds to the middle of the inlet air jet.

It can be noticed that the temperature increase is by about 850 K for the real burner ($A_{air,in} = 88$ mm^2), whereas it is reduced down to 750 K for the largest recirculation degree ($A_{air,in} = 41$ mm^2). The methane self-ignition temperature is 853 K, therefore, according to the criteria by Cavaliere and de Joannon [2] the real burner operation can scarcely be regarded as MILD combustion ("A combustion process is named MILD when the inlet temperature of the reactant mixture is higher than mixture self-ignition temperature whereas the maximum allowable temperature increase with respect to inlet temperature during combustion is lower than mixture self-ignition temperature (in Kelvin)").

For smaller recirculation degree, the temperature increase due to combustion heat release is drastic, for instance being of 1300 K for $A_{air,in} = 339$ mm^2 ($k_R = 23\%$), and reasonably the burner does not operate in MILD combustion mode.

In addition, the shape of temperature profiles obtained for $k_R = 23$ and 59% differs considerably from that obtained with larger recirculation degrees. For large recirculation degrees the high temperature of recirculating exhaust gases increases the mean reactant temperature, leading to temperature profiles characterized by a double peak (Fig. 6). Indeed, the first temperature peak, located at $x = 100$–150 mm, is due to the mixing of fresh reactants with exhaust gases. Conversely, for smaller recirculation degrees ($A_{air,in} = 201$ and 339 mm^2), the contribution of exhaust gases to the reactants' heat capacity is negligible, so that the first temperature peak disappears.

For a better understanding of temperature distributions in the MILD combustion burner, it is useful to analyze radial profiles of temperature at different axial distances along the burner, as reported in Fig. 7. It can be observed that the profiles become less steeper with increasing the recirculation degree, thus confirming more homogeneous temperature distributions. Again, the profiles' shape for the $k_R = 23$ and 59% runs, corresponding to the flame combustion mode, differs strongly from that of the MILD combustion runs.

4.3. Effect of air excess

As mentioned in the Introduction, the experimental campaign was carried out with a relatively high air excess, ensuring an oxygen concentration in the flue gases of 6%. For that reason, simulations were performed also with a smaller air excess of 16%, leading to an oxygen concentration in the exhaust gases of approximately 2.6% (see runs 13 and 14).

It was found that for the same air inlet cross-sectional area $A_{air,in} = 88$ mm^2, the maximum temperature observed in the burner increased from 2080 to 2265 K when the air excess decreased from 46 to 16%. This may be easily imputed to the reduced thermal capacity associated with the recirculating nitrogen. In addition, NO was also found to increase from about 39 to 272 ppm$_v$. Even if the oxygen concentration in the reaction zone diminishes with decreases air excess (see Table 1), thus damping NO formation, the enhanced temperatures govern the NO formation and lead to a strong increase of NO emissions. Therefore, with an air excess of 16%, the standard burner configuration is not sufficient to ensure a completely MILD combustion mode, and larger recirculation degrees would be desirable.

With the smallest air inlet cross-sectional area, $A_{air,in} = 41$ mm^2, and the same air excess of 16%, the NO emissions were found to be reduced down to 58 ppm$_v$.

4.4. Turbulence–chemistry interaction

MILD combustion is typically characterized by a particular kind of turbulence–chemistry interac-

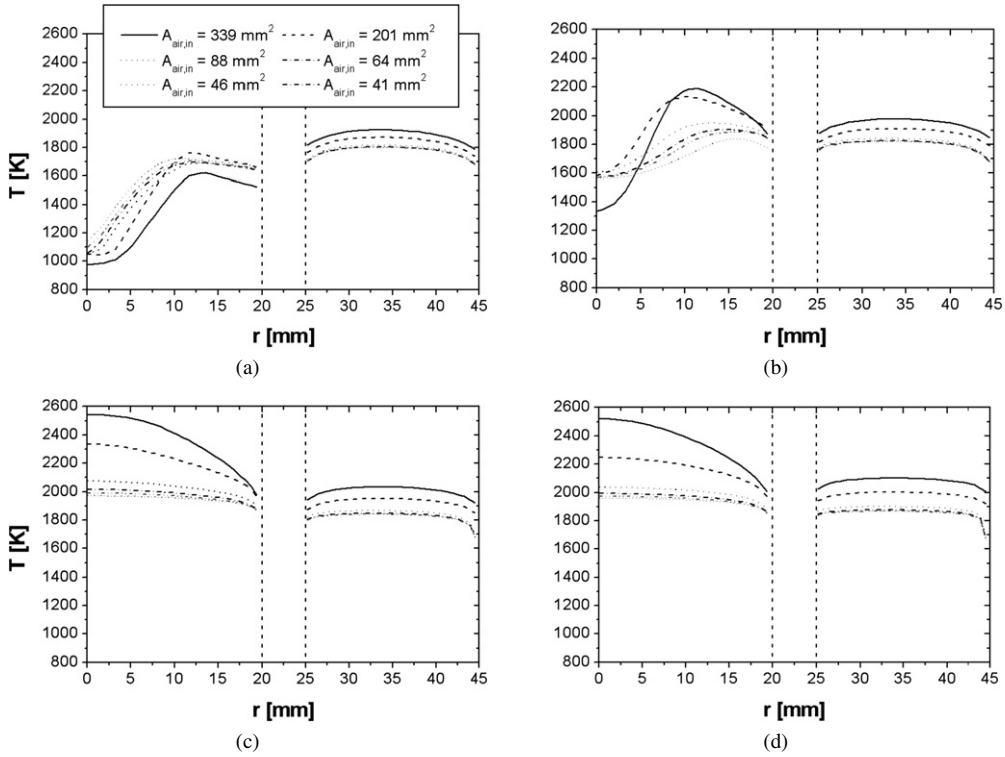

Fig. 7. Radial profiles of temperature for different recirculation degrees under different axial coordinates: (a) $x = 150$; (b) 250; (c) 350; (d) 450 mm. Burner load $\dot{Q}_{\text{in}} = 10.42$ kW (runs 7–12 of Table 1).

tion. Specifically, higher turbulence levels with respect to conventional flames occur in the reaction region because of the strong recirculation, whereas slower chemical rates are observed because of the large dilution of reacting species.

A useful way of estimating the turbulence–chemistry interaction is provided by the Damkohler number, which is the turbulence-to-chemical timescale ratio,

$$\text{Da} = \frac{\tau_{\text{T}}}{\tau_{\text{C}}}. \tag{9}$$

Fig. 8 shows the Damkohler number distribution in the burner through contours for different recirculation degree. The contours have been overlapped to the temperature distribution in the burner in order to facilitate the figure comprehension. Actually, since the chemical timescale is based on one-step kinetics, results cannot provide a quantitative answer but give qualitative evidence of the effect of exhaust gases recirculation on turbulence–chemistry interactions.

Fig. 8a refers to the largest air inlet cross-sectional area, for which the burner is operating in flame mode ($k_{\text{R}} = 23\%$). It can be noticed that the flame front is characterized by large Da values.

Conversely, in Figs. 8b and 8c, that Damkohler number values are low and near unity even in the reaction region, thus proving that both turbulence and chemistry control the reaction rates. This indicates that the combustion model (EDM/FR) used in the present work is conceptually consistent.

Moreover, it can be observed by comparing Fig. 8b and Fig. 8c that regions of higher Damkohler numbers enlarge with increasing the recirculation degree; this is due to the larger turbulence and reactants' dilution.

4.5. Burner efficiency

As mentioned in the introduction, MILD combustion burners are very interesting from an industrial point of view and have been applied to different processes. Therefore it is important to analyze not only their "internal" behavior (e.g., temperature and flow fields) but also their interactions with the surroundings and their performance in terms of thermal efficiency. In particular, recuperative MILD combustion burners enclosed by radiant tubes are widely used in continuous annealing furnaces for electric steel strip. In such applications, it would be desirable to achieve smooth temperature profiles along the radiant tube in order to ensure good steel quality and safe conditions for the material constituting the radiant tube. Therefore, local temperature peaks and gra-

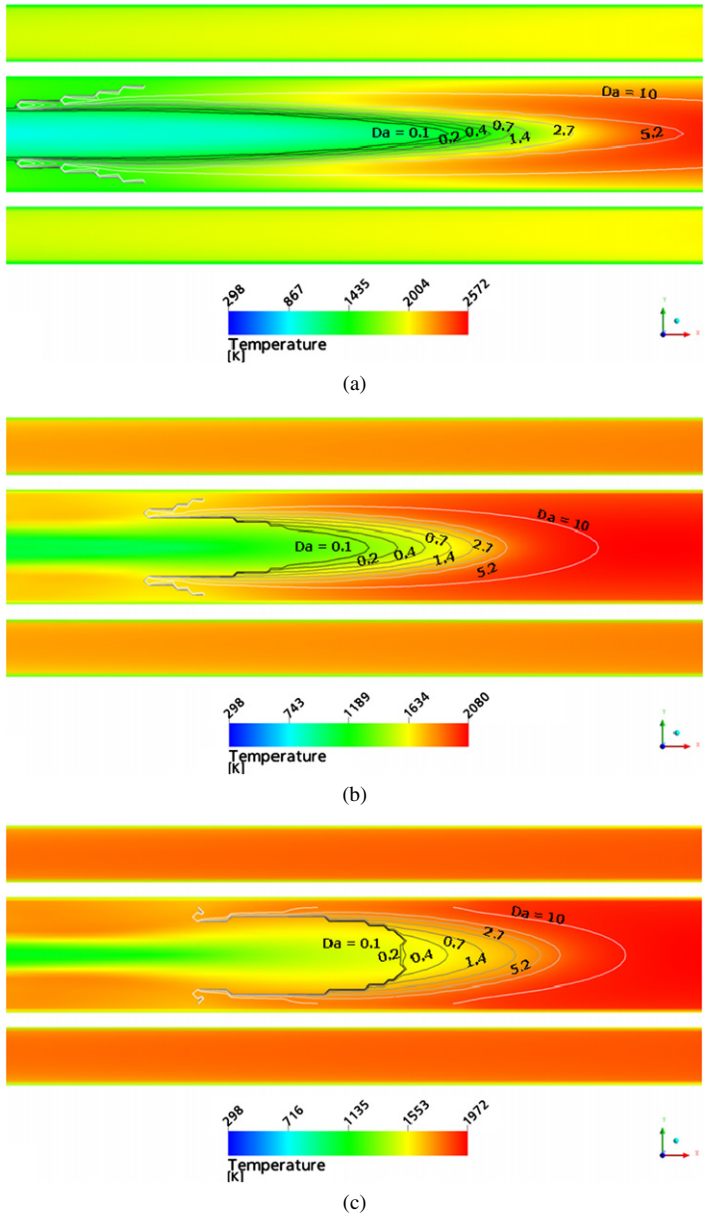

Fig. 8. Temperature (colored map) and Damkohler number (contours) distributions for (a) $A_{\mathrm{air,in}} = 339\ \mathrm{mm}^2$; (b) $A_{\mathrm{air,in}} = 88\ \mathrm{mm}^2$; (c) $A_{\mathrm{air,in}} = 46\ \mathrm{mm}^2$. Burner load $\dot{Q}_{\mathrm{in}} = 10.42$ kW (runs 8, 7, 11 of Table 1).

dients should be minimized to avoid the collapse of the radiant tube itself due to localized phenomenona, such as deformation and mechanical stresses arising from nonuniform thermal expansion [29].

Fig. 9 shows temperature profiles along the radiant tube for a burner load of 10.42 kW and different values of the recirculation degrees. A large temperature interval, greater than 230 K, is observed for the flame combustion mode, whereas in the MILD combustion regime the temperature profiles appear more uniform, covering temperature intervals of about 150 K. Therefore this condition is more suited to ensure homogeneous conditions.

Another criterion to evaluate the burner performance is based on the thermal efficiency. In particular two different efficiencies can be calculated: a radiation efficiency based on heat transfer from the radiant tube and a recovery efficiency characterizing the air preheater performance. The former efficiency may be calculated as

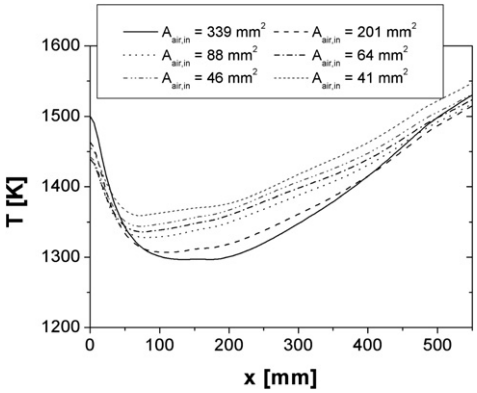

Fig. 9. Radiant tube temperature as a function of the air inlet cross-sectional area. Burner load $\dot{Q}_{\text{in}} = 10.42$ kW (runs 7–12 of Table 1).

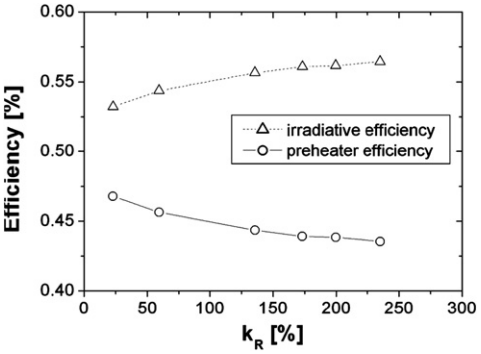

Fig. 10. Preheater and radiant rube efficiencies as a function of the recirculation degree. Burner load $\dot{Q}_{\text{in}} = 10.42$ kW (runs 7–12 of Table 1).

$$\eta_{\text{rad}} = \frac{\dot{Q}}{\dot{Q}_{\text{in}}}, \tag{10}$$

whereas the recovery efficiency is

$$\eta_{\text{rec}} = \frac{\dot{Q}_{\text{rec}}}{\dot{Q}_{\text{in}}}. \tag{11}$$

Fig. 10 shows the two efficiencies as a function of the recirculation degree. It is worth noting that the sum of the two efficiencies approaches unity as in the type of burner works through (mainly irradiative) heat losses towards the surroundings. It can be also observed that the radiation efficiency increases with increasing recirculation degree; thus the burner ensures better performances in the MILD combustion regime than in the flame mode.

4.6. Comparison of axisymmetric and 3-dimensional simulations

As mentioned earlier, simulations of recuperative MILD combustion burners available in the literature

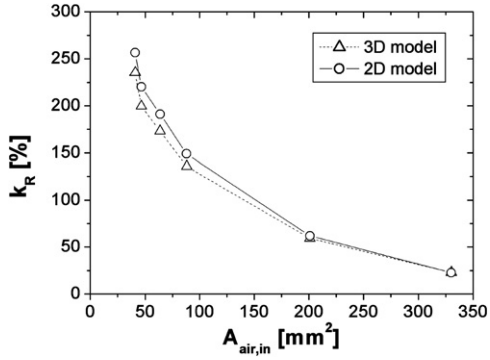

Fig. 11. Recirculation degree as a function of the air inlet cross-sectional area predicted with the axisymmetric and 3-dimensional models. Burner load $\dot{Q}_{\text{in}} = 10.42$ kW (runs 7–12 of Table 1).

are 2-dimensional simulations [19,20]. Therefore the presence of the three recirculation windows is usually neglected.

In the present work axisymmetric simulations were also performed and compared to the 3-dimensional simulations in order to estimate the effect of the recirculation windows, as well as errors arising when they are not taken into account.

Axisymmetric simulations will be denoted as "2D" for brevity, even if, strictly speaking, they are not 2-dimensional simulations, the computational domain corresponding to a 5° angular sector (see description of computational domain given in Section 3).

Fig. 11 indicates that recirculation degrees predicted through the axisymmetric model are larger than those predicted through the 3-dimensional model by 15–20% for the smallest air inlet cross-sectional areas. This is reasonable, as in axisymmetric models the exhaust gases' recirculation into the reaction zone is facilitated by the larger, i.e., 360° opening. For the largest air inlet cross-sectional areas, corresponding to the flame mode operations, there is little difference between the 3-dimensional simulation and the axisymmetric model; this may be partly imputed to the small value of predicted recirculation degrees, which makes differences negligible.

Because of the larger predicted recirculation degrees, 2-dimensional models are expected to underestimate NO emissions, as confirmed by Fig. 12.

However, results obtained with the two approaches (2D vs 3D) could be fitted by the same regression curve when reported as functions of the recirculation degree (see Fig. 13), suggesting that the relation between NO formation and exhaust gas recirculation remains the same.

The best regression law was found to be the Boltzmann sigmoidal regression

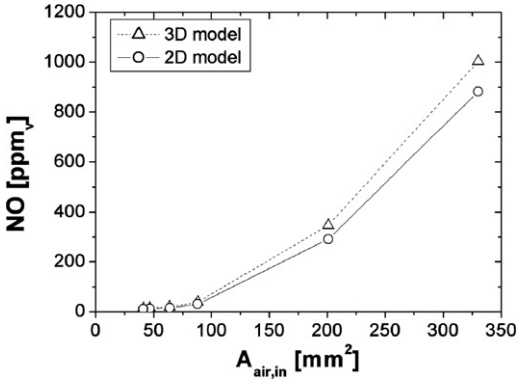

Fig. 12. NO emissions as a function of the air inlet cross-sectional area predicted with the axisymmetric and 3-dimensional models. Burner load $\dot{Q}_{\text{in}} = 10.42$ kW (runs 7–12 of Table 1).

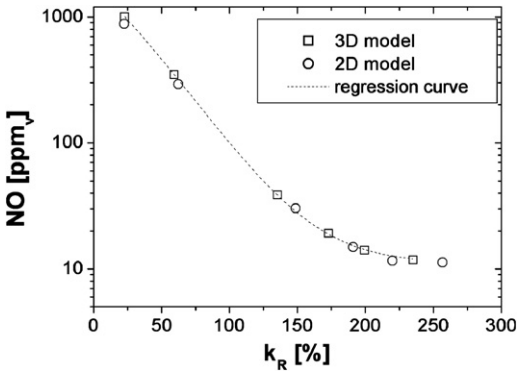

Fig. 13. NO emissions as a function of the recirculation degree predicted with the axisymmetric and 3-dimensional models. Burner load $\dot{Q}_{\text{in}} = 10.42$ kW (runs 7–12 of Table 1).

$$X_{\text{NO}} = \frac{X_{\text{NO\_1}} - X_{\text{NO\_2}}}{1 + e^{k_R - k_{R_0}/\Delta k}} + X_{\text{NO\_2}}, \tag{12}$$

with $X_{\text{NO\_1}} = 0.00553$, $X_{\text{NO\_2}} = 0.00001$, $k_{\text{R0}} = -22.3\%$, and $\Delta k = 29.8\%$, and a root mean squared error approximating unity.

Therefore axisymmetric simulations could be performed, allowing lower computational cost, and predicted NO corrected by assuming 15–20% larger recirculation degrees.

Nevertheless, it is worth noting that a more accurate observation of the burner temperature and velocity distribution indicates that axisymmetric and 3-dimensional simulations differ substantially. This is evident from Fig. 14, which compares radial temperature profiles obtained with the two models for different axial coordinates and recirculation degrees.

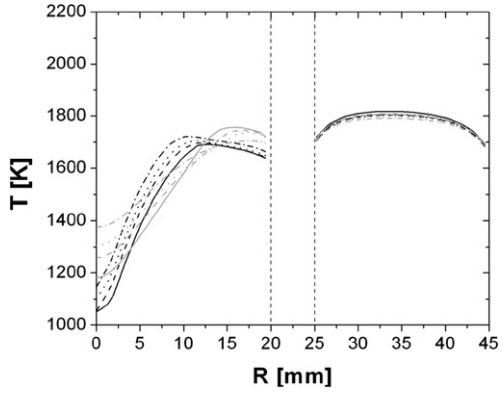

(a)

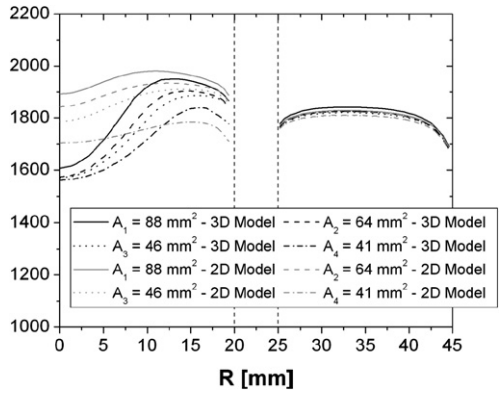

(b)

Fig. 14. Radial profiles of temperature for different recirculation degrees and for axisymmetric and 3-dimensional models at different axial coordinates: (a) $x = 150$; (b) 250 mm. Burner load $\dot{Q}_{\text{in}} = 10.42$ kW (runs 7, 10, 11, and 12 of Table 1).

5. Conclusions

A numerical investigation through computational fluid dynamics of a recuperative MILD combustion burner operating in MILD combustion mode has been presented.

The numerical model contained two subroutines: the first subroutine models the air preheater, whereas the second subroutine is aimed at modeling irradiative heat losses from the burner toward the surroundings. Importantly, in this manner the burner model was self-sufficient, which means it did not need any assumptions (e.g., on the air inlet temperature).

Because of its complexity, the CFD model was assessed through comparison with experimental data, concerning temperature profiles along the outer surfaces of the burner and species concentration in the flue gases. It is noteworthy that only global data and measurements taken on the outer surfaces of the burner were available, as the burner is a real industrial burner. Local data would be desirable, but the

burner does not allow any access to its interior for the measurements. Besides, the complexity of the CFD model and the need for subroutines arose partly from the wish to model the burner without any additional assumptions, trying to exploit all the available measurements (e.g., temperature along the radiant tube).

The burner was observed to produce about 30 ppm_v of NO in flameless mode. For the same air-preheating the burner would have produced about 1000 ppm_v of NO in flame mode. In addition, it was found that the burner performance in terms of thermal efficiency improved when it was operated in MILD combustion mode. The temperatures on the outer surface of the burner were also more homogeneous, ensuring more uniform conditions, which are beneficial for many process such as steel annealing processes.

A further reduction of the air injection nozzles was also investigated in order to promote recirculation of exhaust gases by increasing the air inlet jet momentum and suppressing further NO emissions. In particular, NO emissions of just 10 ppm_v were produced by halving the air inlet cross-sectional area.

The analysis of turbulence and chemical timescales confirmed that in MILD combustion the high-temperature region is characterized by Damkohler numbers lower than those observed in the flame front of the burner operating in flame mode. Therefore the importance of the turbulence–chemistry interaction treatment was confirmed.

Finally, two geometrical models of the burner have been compared: a 3-dimensional model and an axisymmetric model. This latter model is usually preferred to the former in the available literature for the modeling of MILD combustion burners, because of its lower computational cost. It was found that the axisymmetric model overestimates the recirculation degree in the burner by 15–20%, and thus underpredicts NO emissions. However, for engineering purposes, a satisfactory prediction of NO emissions could be achieved by extrapolating data from the NO concentration versus the recirculation degree curve and considering a lower recirculation degree than that predicted through the axisymmetric model. However, temperature and flow fields obtained with the axisymmetric model should be handled carefully.

In conclusion, the careful application of commercial codes with detailed analysis of different modeling hypotheses is able to give a satisfactory view of the most important effects of MILD combustion. In particular, in industrial conditions, where the burner structure and the characteristics of the experimental tests do not make it possible to take detailed local measurement within the reacting system, the approach followed describes the main features of the reacting system, at least from an engineering point of view.

Acknowledgment

The authors thank Enel Ricerca Laboratories of Livorno, Italy, for support in the experimental campaign.

References

[1] J.A. Wünning, J.G. Wünning, Prog. Energy Combust. Sci. 23 (1997) 81–94.
[2] A. Cavaliere, M. de Joannon, Prog. Energy Combust. Sci. 30 (2004) 329–366.
[3] A. Cavigiolo, M.A. Galbiati, A. Effuggi, D. Gelosa, R. Rota, Combust. Sci. Technol. 175 (2003) 1347–1367.
[4] M. de Joannon, A. Cavaliere, T. Faravelli, E. Ranzi, P. Sabia, A. Tregrossi, Proc. Combust. Inst. 30 (2005) 2605–2612.
[5] A. Milani, A. Saponaro, IFRF Combust. J. 200101 (2001).
[6] G.M. Choi, M. Katsuki, Energy Convers. Manage. 42 (2001) 639–652.
[7] M. Flamme, Energy Convers. Manage. 42 (2001) 1919–1935.
[8] M. Flamme, Appl. Therm. Eng. 24 (2004) 1551–1559.
[9] Y.D. Wang, Y. Huang, D. Mcllveen-Wright, J. McMullan, N. Hewitt, P. Eames, S. Rezvani, Fuel Process. Technol. 87 (2006) 727–736.
[10] S. Kumar, P.J. Paul, H.S. Mukunda, Proc. Combust. Inst. 30 (2005) 2613–2621.
[11] P.J. Coelho, N. Peters, Combust. Flame 124 (2001) 503–518.
[12] T. Plessing, N. Peters, J.G. Wünning, Proc. Combust. Inst. 27 (1998) 3197–3204.
[13] B.I. Özdemir, N. Peters, Exp. Fluids 30 (2001) 683–695.
[14] B.B. Dally, E. Riesmeier, N. Peters, Combust. Flame 137 (2004) 418–431.
[15] S. Orsino, R. Weber, U. Bollettini, Combust. Sci. Technol. 170 (2001) 1–34.
[16] F.C. Christo, B.B. Dally, Combust. Flame 142 (2005) 117–129.
[17] B.B. Dally, A.N. Karpetis, R.S. Barlow, Proc. Combust. Inst. 29 (2002) 1147–1154.
[18] B.F. Magnussen, B.H. Hjertager, Combust. Inst. 16 (1976) 719–729.
[19] E. Malfa, M. Venturino, V. Tota, 25th Event of the Italian Section of the Combustion Institute, Rome, June 3–5, 2002.
[20] A. Al-Halbouni, A. Giese, M. Flamme, M. Brune, Clean Air 5 (2004) 391–405.
[21] A.P. Morse, Axisymmetric turbulent shear flows with and without Swirl, Ph.D. thesis, London University, 1977.
[22] T.F. Smith, Z.F. Shen, J.N. Friedman, J. Heat Transfer 104 (1982) 602–608.
[23] C.K. Westbrook, F.L. Dryer, Combust. Sci. Technol. 27 (1981) 31–43.
[24] A.A. Westenberg, Combust. Sci. Technol. 4 (1971) 59–64.

[25] G.G. De Soete, Proc. Combust. Inst. 15 (1974) 1093–1102.
[26] M. Missaghi, Mathematical modelling of chemical sources in turbulent combustion, Ph.D. thesis, The University of Leeds, England, 1987.
[27] J.C. Slattery, R.B. Bird, AIChE J. 42 (1958) 137–142.
[28] S.P. Wilke, J. Comput. Phys. 18 (1950) 517–519.
[29] A. Milani, J.G. Wünning, IFRF Combust. J. 200405 (2004).